
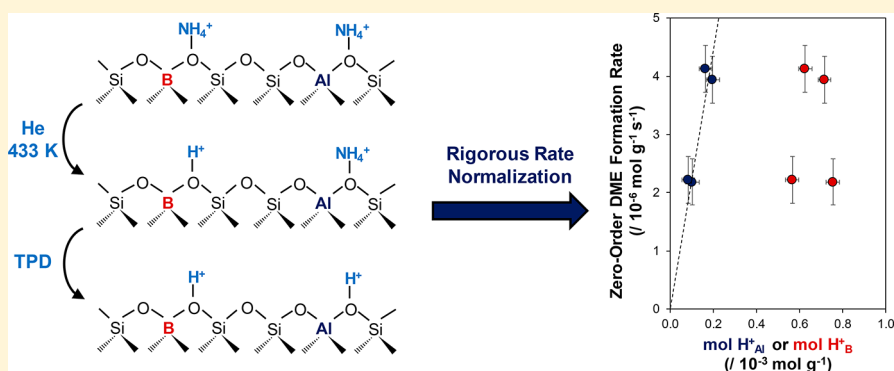


Ammonia Titration Methods To Quantify Brønsted Acid Sites in Zeolites Substituted with Aluminum and Boron Heteroatoms

Philip M. Kester, Jeffrey T. Miller, and Rajamani Gounder*

Charles D. Davidson School of Chemical Engineering, Purdue University, 480 Stadium Mall Drive, West Lafayette, Indiana 47907, United States

 Supporting Information



ABSTRACT: Ammonia titration methods were developed to discriminate and quantify Brønsted acid sites of different strength that compensate aluminum and boron heteroatoms incorporated within zeolite frameworks. Borosilicate and boroaluminosilicate MFI zeolites (B-Al-MFI) were synthesized with different Al contents and crystallite sizes, which are typically correlated structural properties in aluminosilicates synthesized hydrothermally, but independently varied here by incorporating boron as a second framework heteroatom and using ethylenediamine as a structure directing agent. Temperature-programmed desorption (TPD) of ammonia from B-Al-MFI samples saturated via liquid-phase NH₄NO₃ ion exchange resulted in quantifying the total number of Al and B heteroatoms. In contrast, TPD performed after NH₄-form B-Al-MFI samples were purged in flowing helium (433 K), or after gas-phase NH₃ adsorption (433 K) onto H-form B-Al-MFI samples, quantified only protons charge-compensating framework Al heteroatoms. Turnover rates for methanol dehydration to dimethyl ether, when measured in zero-order kinetic regimes that are sensitive predominantly to Brønsted acid strength, are dependent only on the number of protons compensating framework Al atoms in B-Al-MFI zeolites. The NH₃ titration methods developed here are useful in rigorously normalizing turnover rates of Brønsted acid-catalyzed reactions in boroaluminosilicate zeolites, which have been recognized previously to be dependent solely on Al content. The incorporation of B heteroatoms into zeolite frameworks, which generate protons that are essentially unreactive, provides a strategy to influence crystallite sizes independently of Al content, especially relevant in cases where catalytic behavior is influenced by intracrystalline transport phenomena.

1. INTRODUCTION

Aluminosilicate zeolites are a class of solid Brønsted acid catalysts that are widely used in petrochemical refining,^{1,2} of which the MFI framework has received particular attention for converting methanol³ and alkenes (C₂–C₁₂)^{4,5} into heavier molecular weight compounds used as transportation fuels. Crystallite sizes and framework Al content influence the reactivity, selectivity, and deactivation of MFI zeolites in methanol-to-olefins^{6–9} and alkene oligomerization^{10–12} catalysis, because longer diffusion paths and higher Al contents preferentially increase intracrystalline residence times of larger products, increasing their propensity to undergo secondary reactions to form smaller molecules that egress more readily from intracrystalline pore networks. The combined effects of crystallite size and framework Al content are reflected in a characteristic diffusion parameter (Ψ) within Thiele modulus expressions, proportional to the

square of the characteristic diffusion length and to the volumetric acid site density of a given crystallite, as used by Sarazen and Iglesia to interpret changes in propene oligomerization product selectivities on different Al-MFI zeolites.¹² The location of Brønsted acidic protons among the intraporous voids present in MFI, which is dependent on the distribution of Al atoms among crystallographically distinct tetrahedral site (T-site) positions, also influences reactivity and selectivity.¹³ In the case of propene dimerization, turnover rates are dependent on the geometry of pore structures confining Brønsted acid sites, which determine the strength of van der Waals interactions between lattice oxygen

Received: March 1, 2018

Revised: April 20, 2018

Accepted: April 24, 2018

Published: April 24, 2018

atoms and carbenium ion transition states stabilized at such sites.¹⁴ In the case of methanol-to-olefin reactions that occur via a hydrocarbon pool mechanism,^{3,15} larger channel intersections in MFI (and MWW) zeolites have been reported to preferentially stabilize larger transition states of aromatic-based cycles, while smaller 10-membered ring (10-MR) channels do so for smaller transition states in olefin-based cycles.^{16,17} As a result, synthetic methods to prepare MFI zeolites with varying crystallite size, and framework Al content and distribution,^{16,18} can generate materials with different catalytic properties for a variety of hydrocarbon upgrading processes.¹³

Crystallite sizes tend to increase with decreasing Al content among MFI zeolites crystallized hydrothermally in the presence of tetrapropylammonium (TPA⁺) cations,^{19–21} although using diquaternary ammonium surfactants can restrict crystal growth to form single-unit-cell-thick zeolite sheets,⁷ and using zeolite growth modifiers that selectively bind to certain crystal facets can inhibit crystal growth in certain dimensions.^{22,23} The synthesis of boroaluminosilicate MFI (B-Al-MFI) zeolites from mixtures containing equimolar quantities of B and Al has been reported to produce smaller crystallites ($\sim 6\ \mu\text{m}$) than aluminosilicate MFI zeolites ($\sim 10\ \mu\text{m}$) at fixed Al content (Si/Al = 12).^{24–27} Al, ²⁹Si, and ¹¹B magic angle spinning nuclear magnetic resonance (MAS NMR) spectroscopy has provided evidence that B competes with Al for incorporation at certain T-sites in MFI, resulting in changes to the Al distribution among different possible T-sites at a given Si/Al ratio.²⁵ Similar effects of B incorporation on the resulting Al distribution have been reported in MCM-22, using infrared (IR) spectroscopy of adsorbed pyridine (after protons in supercages and surface pockets were selectively poisoned by *m*-xylene) and ²⁷Al NMR to identify acid sites in smaller 10-MR sinusoidal channels,¹⁷ which are less prone to deactivation by carbonaceous deposits during methanol-to-hydrocarbons catalysis than acid sites in larger voids. Although B competes with Al for incorporation in siliceous frameworks, their corresponding bridging OH groups are much weaker in Brønsted acid strength, reflected in deprotonation energies (DPE) that are $\sim 70\ \text{kJ mol}^{-1}$ greater than bridging OH groups at framework Al.²⁶ Such large differences in deprotonation energy result in zero-order rate constants of methanol dehydration to dimethyl ether, which are dependent predominantly on acid strength and are essentially insensitive to confinement effects,²⁷ estimated to be an order of magnitude higher (per H⁺, 433 K) on Al-MFI than B-MFI.²⁶ Rates (per g) of other Brønsted acid-catalyzed reactions (*n*-hexane cracking,²⁸ ethylbenzene dealkylation,²⁸ cyclopropane isomerization,²⁸ ethylene methylation²⁵) in B-Al-MFI samples have been reported to correlate with their total number of Al sites (per g), even when present in trace quantities ($<100\ \text{ppm Al}$, Al/B < 0.01) that are introduced, in certain cases, as adventitious impurities from silica precursors²⁹ or alumina binders.^{28,30} Thus, the incorporation of boron as a noncatalytic heteroatom in Brønsted acidic zeolites provides a strategy to influence crystallite size independently of framework Al content and distribution.

Interpreting catalytic phenomena of Brønsted acidic origin on boroaluminosilicates, especially in the normalization of rate data, requires methods to discriminate and quantify protons compensating framework Al and B. Previous methods to identify framework Al in boroaluminosilicates have used ²⁷Al, ²⁹Si, and ¹¹B MAS NMR spectroscopy,^{17,25,31} although ²⁷Al MAS NMR characterization of aluminosilicates can overestimate the number of Brønsted acidic protons, because tetrahedral Al species detected in NMR spectra are structural proxies for the number of proton active sites present during reaction.^{32–34} Moreover, B

atoms trigonally coordinated within *BEA frameworks have been reported to appear as tetrahedral in ¹¹B MAS NMR spectra, depending on the extent of sample hydration.³⁵ IR OH stretching vibrations of protons at framework Al and B have been observed at ~ 3600 and $\sim 3700\ \text{cm}^{-1}$,^{25,36,37} respectively, but have not been directly quantified to our knowledge in boroaluminosilicates, which would require independent molar extinction coefficients for the two OH groups. Temperature-programmed desorption (TPD) of bases often results in a multitude of desorption features, as observed for ammonia desorption and attributed to acid strength differences between protons compensating framework B and Al.^{17,25,38,39} Yet, ambiguities in interpreting the position of desorption features on the basis of binding strength exist because of convoluting effects of molecular readsorption and diffusion phenomena during egress from microporous voids.^{40,41} Gorte and co-workers have shown that alkylamine titrants (*t*-butylamine, *i*-propylamine) undergo Hoffman elimination to form ammonia and the corresponding alkene at protons associated with framework Al, but desorb intact from OH groups formed from framework B,^{42,43} suggesting that such methods could distinguish framework Al and B.

Here, we adapt strategies reported previously for using ammonia titrants to discriminate and quantify sites of different binding strength that arise from Brønsted and Lewis acid sites that coexist in H-form⁴⁴ and partially Cu-exchanged^{34,45} aluminosilicates, in order to do so for protons of different Brønsted acid strength generated from framework B and Al in boroaluminosilicates. Titration methods using ammonia are especially useful to quantify protons in porous materials of certain topology (e.g., small-pore frameworks³⁴) or composition (low Si/Al with protons in close proximity³²) that present challenges when using bulkier alkylamine titrants. We provide evidence that TPD of ammonia after liquid-phase ion exchange to saturation allows quantification of all framework Al and B heteroatoms (either trigonal or tetrahedral³⁷), while methods to purge weakly bound ammonia (433 K, He) from framework B allow quantification of only protons at framework Al sites (H⁺_{Al}) in a subsequent TPD. Gas-phase ammonia saturation of H-form B-Al-MFI samples at 433 K provides identical quantification in a subsequent TPD, because ammonia does not adsorb to protons at framework B under these conditions. These proton site quantifications are useful in normalizing rates of Brønsted acid-catalyzed reactions on boroaluminosilicates, verified here by measuring zero-order rate constants for methanol dehydration to dimethyl ether, a catalytic probe that is sensitive to acid strength and can discriminate catalytic contributions from protons at Al and B in zeolite frameworks.²⁶

2. MATERIALS AND METHODS

2.1. Catalyst Synthesis and Preparation. B-Al-MFI zeolites were synthesized from solutions with molar ratios of 1 SiO₂/0.3 EDA/X H₃BO₃/Y Al(NO₃)₃/0.01 TPABr/10.2 H₂O, with values of X ranging from 0.08 to 0.40 and values of Y ranging from 0.006 to 0.012. All samples are denoted B-Al-MFI (Si/B, Si/Al), where Si/B and Si/Al correspond to the molar ratios present in the synthesis solutions. Ethylenediamine (99.5 wt %, Sigma-Aldrich, EDA) was first diluted with deionized water (18.2 MΩ) in a perfluoroalkoxy alkane (PFA) container (Saville Corp.), followed by the addition of boric acid (99.5 wt %, Sigma-Aldrich). This solution was mixed for 15 min under ambient conditions. A separate mixture of aluminum nitrate nonahydrate (98 wt %, Sigma-Aldrich) and tetra-*n*-propylammonium bromide (98 wt %, Alfa Aesar) in deionized water was

also mixed for 15 min under ambient conditions. The two solutions were then combined into one PFA container, followed by the addition of colloidal silica (Ludox HS40, 40 wt %, Sigma–Aldrich). This mixture was then stirred under ambient conditions for 2 h to produce a homogeneous solution, added to a 45 mL Teflon-lined stainless steel autoclave (Parr Instruments), and heated in a forced convection oven (Yamato DKN-402C) at 448 K under rotation at 40 rpm for 5 days.

B-MFI zeolites were synthesized from solutions with molar ratios of 1 SiO₂/0.3 EDA/X H₃BO₃/0.01 TPABr/10.2 H₂O, with values of *X* ranging from 0.08 to 0.40. Samples are denoted B-MFI (Si/B), where Si/B corresponds to the molar ratio present in the synthesis solution. Ethylenediamine (99.5 wt %, Sigma–Aldrich) was first diluted with deionized water (18.2 MΩ) in a PFA container, followed by the addition of boric acid (99.5 wt %, Sigma–Aldrich). This solution was mixed for 15 min under ambient conditions. A separate mixture of tetra-*n*-propylammonium bromide (98 wt %, Alfa Aesar) in deionized water was also mixed for 15 min under ambient conditions. The two solutions were then combined into one PFA container, followed by addition of tetraethylorthosilicate (98 wt %, Sigma–Aldrich, TEOS) and stirred for 2 h uncovered and under flowing air to evaporate the ethanol evolved from hydrolysis of TEOS. The mixture was then added to a 45 mL Teflon-lined stainless steel autoclave (Parr Instruments), heated in a forced convection oven (Yamato, Model DKN-402C) at 448 K under rotation at 40 rpm for 5 days.

Solid products were removed from the Teflon liners and washed with water and acetone (Sigma–Aldrich, >99.5 wt %) in alternating washes (30 cm³ (g solid)^{−1} per wash) until the pH of the supernatant solution was constant. Solids were separated by centrifugation, dried in air at 373 K for 24 h, and then treated in flowing dry air (1.67 cm³ s^{−1} (g solid)^{−1}, UHP, 99.999%, Indiana Oxygen) to 853 K (0.0167 K s^{−1}) and held for 10 h in a muffle furnace (Nabertherm L/E 611 with a P300 controller) to remove organic structure directing agents from zeolite products.

B-Al-MFI and B-MFI samples were converted to their NH₄ form by aqueous-phase ion exchange (100 cm³ (g solid)^{−1}) in a 1.0 M NH₄NO₃ solution (8.0 wt % in deionized H₂O; 99.9 wt %, Sigma–Aldrich) for 24 h under ambient conditions, then washed with deionized water (70 cm³ per g solids), recovered via centrifugation, and dried in air at 373 K for 24 h. NH₄-form samples were converted to their H form by treatment in flowing dry air (1.67 cm³ s^{−1} (g solid)^{−1}, UHP, 99.999%, Indiana Oxygen) to 773 K (0.0167 K s^{−1}) for 4 h in a muffle furnace (Nabertherm L/E 611 with a P300 controller).

2.2. Characterization of B-Al-MFI and B-MFI. Crystal structures were verified with powder X-ray diffraction (XRD) patterns collected using a Rigaku SmartLab X-ray diffractometer with a Cu Kα source operating at 1.76 kW. Typically, 0.01 g of sample was loaded into a zero-background, low-dead-volume sample holder (Rigaku) and diffraction patterns were measured from 4° to 40° at a scan rate of 0.0167° s^{−1} and a step size of 0.01°.

Micropore volumes were calculated from N₂ adsorption isotherms measured at 77 K with a Micromeritics ASAP 2020 surface area and porosity analyzer. B-MFI and B-Al-MFI samples (0.04–0.06 g, sieved to 180–250 μm) were degassed by heating to 393 K (0.167 K s^{−1}) under vacuum (5 μmHg) for 2 h, then further heating to 623 K (0.167 K s^{−1}) under vacuum (<5 mmHg) and holding for 9 h. The linear volumetric uptake of N₂ (for 0.05–0.35 *P/P*₀) was used to estimate micropore volumes (cm³ (g solid)^{−1} at STP). These results were compared to those

from a semilogarithmic derivative plot of the isotherm, given by $\partial(V_{\text{ads}})/\partial(\ln(P/P_0))$ vs $\ln(P/P_0)$. The volume of N₂ adsorbed at the first minimum in this plot corresponds to the point at which the micropores have been filled, from which micropore volumes were calculated.^{46,47} All reported micropore volumes agreed (±10%) between these two methods.

Elemental analysis of aluminum in B-MFI and B-Al-MFI zeolites were performed via atomic absorption spectroscopy (AAS) with a PerkinElmer Model AAnalyst 300 atomic absorption spectrometer. Samples were prepared by dissolving 0.04 g of solid in 2 g of hydrofluoric acid (48 wt %, Alfa Aesar) and allowed to sit overnight, then diluted in 50 g of deionized water (18.2 MΩ). [**Caution: when working with HF acid, use appropriate personal protective equipment, ventilation, and other safety precautions.**] Absorbances were measured with radiation sources at wavelengths of 309.3 nm in a reducing acetylene/nitrous oxide flame. Elemental compositions were calculated using calibration curves generated from known solutions. Silicon and boron contents in B-Al-MFI were determined by inductively coupled plasma–optical emission spectroscopy (ICP-OES) (Galbraith Laboratories).

Images were collected via scanning electron microscopy (SEM) on an FEI Quanta 3D FEG Dual-beam SEM system. Prior to imaging, samples were coated with platinum to reduce charging. Images were taken at an accelerating voltage of 15 kV and spot size of 6 μm at 3500×–50 000× magnification.

2.3. Temperature-Programmed Desorption. TPD experiments were performed with a Micromeritics AutoChem II 2920 Chemisorption analyzer and an Agilent 5973N mass-selective detection (MSD) system to identify the gaseous products evolved from zeolite samples. MFI samples (0.04–0.08 g, sieved to 180–250 μm) were supported between two quartz wool plugs in a U-shaped quartz cell and placed in a clam-shell furnace. Calibration and deconvolution methods were performed according to previous reports.⁴⁵

The total number of Al and B sites was estimated by holding NH₄-form B-Al-MFI samples at 323 K for 0.5 h under flowing helium (15 cm³ s^{−1} (g solid)^{−1}, UHP, 99.999%, Indiana Oxygen), followed by increasing the temperature to 873 K (0.167 K s^{−1}) while the effluent gas was sent to the MSD system for analysis.

Two additional methods were used to titrate only protons at framework Al in B-Al-MFI. In the first method, NH₄-form samples were held under flowing helium (15 cm³ s^{−1} (g solid)^{−1}, UHP, 99.999%, Indiana Oxygen), heated to 433 K (0.167 K s^{−1}), and held isothermally for 4 h. The temperature was then increased to 873 K (0.167 K s^{−1}) while the effluent gas was sent to the MSD system for analysis.

In the second method, prior to gas-phase NH₃ saturation, H-form B-Al-MFI samples were treated in flowing dry air (15 cm³ s^{−1} (g solid)^{−1}, UHP, 99.999%, Indiana Oxygen) to 673 K (0.167 K s^{−1}) and held for 2 h, then cooled to 433 K under flowing helium (15 cm³ s^{−1} (g solid)^{−1}) and held for 1 h. Samples were then saturated with gaseous NH₃ (30 cm³ s^{−1} (g solid)^{−1}, 500 ppm of NH₃ in helium, Indiana Oxygen) for 2 h, then held isothermally in flowing helium (15 cm³ s^{−1} (g solid)^{−1}) for 4 h. The temperature was then increased to 873 K (0.083 K s^{−1}) while the effluent gas was sent to the MSD system for analysis.

2.4. Methanol Dehydration Kinetic Measurements. Methanol dehydration rates were measured under differential conversions (<10%) in a tubular packed-bed quartz reactor (7 mm inner diameter) with H-B-Al-MFI samples (0.02–0.03 g, sieved to 180–250 μm) supported between two quartz wool plugs. Reaction temperatures were controlled in a resistively

Table 1. Physiochemical Properties and Elemental Compositions of B-Al-MFI and B-MFI Zeolites

sample ^a	solid Si/Al ^b	solid Si/B ^c	B/EDA in synthesis	micropore volume ^d (cm ³ g ⁻¹)	characteristic length (μm)	diffusion parameter (mol H ₂ ⁺ nm ⁻¹)
B-Al-MFI (2.6, 176)	142	32	1.33	0.13	0.3	0.02
B-Al-MFI (2.6, 88)	88	30	1.33	0.13	0.4	0.07
B-Al-MFI (13, 176)	153	30	0.26	0.13	8.9	15
B-Al-MFI (13, 88)	74	35	0.26	0.15	10.7	42
B-MFI (2.6)	n.d. ^e	n.d. ^e	1.33	0.14	0.3	n.d. ^e
B-MFI (13)	n.d. ^e	n.d. ^e	0.26	0.13	1.0	n.d. ^e

^aSamples are denoted B-Al-MFI (Si/B, Si/Al) and B-MFI (Si/B), where Si/B and Si/Al correspond to the molar ratios present in the synthesis solutions. ^bDetermined from atomic absorption spectroscopy. Errors are $\pm 10\%$. ^cDetermined from ICP-OES. Errors are $\pm 10\%$. ^dErrors are ± 0.01 cm³ g⁻¹. ^eNot determined.

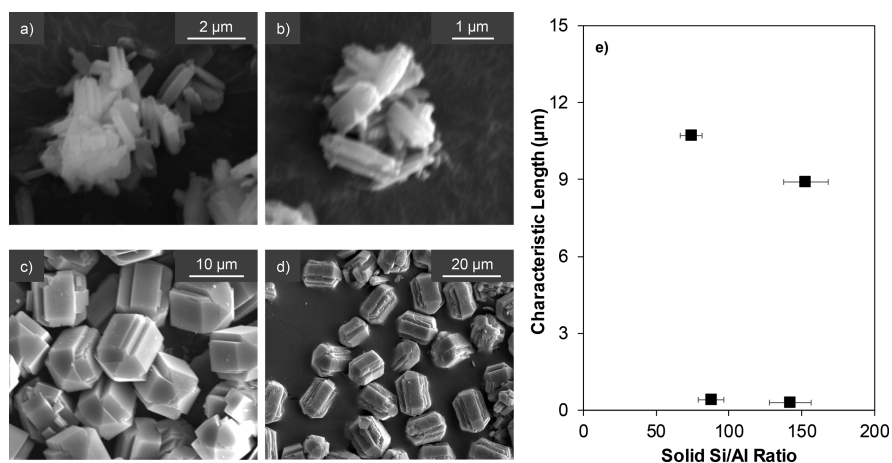


Figure 1. SEM micrographs of (a) B-Al-MFI (2.6, 176), (b) B-Al-MFI (2.6, 88), (c) B-Al-MFI (13, 176), and (d) B-Al-MFI (13, 88). (e) Plot of characteristic crystallite lengths and Si/Al ratio of solid B-Al-MFI products formed.

heated three-zone furnace (Applied Test Systems Series 3210) and Watlow controllers (EZ-Zone series). Catalyst temperatures were measured with a Type K thermocouple placed at the external surface of the quartz tube at the middle of the catalyst bed. Methanol (99.9 wt %, Sigma–Aldrich) partial pressures were controlled with a syringe pump (Legato 100, KD Scientific) and injected into a stream of flowing helium (UHP, 99.999%, Indiana Oxygen) and transferred to the reactor via heated lines maintained at >373 K using resistive heating tape (BriskHeat Co.) and insulating wrap. H-B-Al-MFI samples were first treated in flowing 5% O₂ with a balance of helium ($50 \text{ cm}^3 \text{ s}^{-1}$ (g solid)⁻¹, 99.999%, Indiana Oxygen) to 773 K (0.033 K s^{-1}) and held for 4 h before cooling to 415 K under a helium flow ($150 \text{ cm}^3 \text{ s}^{-1}$ (g solid)⁻¹) prior to rate measurements. Methanol partial pressures in the reactant stream were measured in a bypass configuration. Concentrations of reactants and products were measured with a gas chromatograph that was equipped with a flame ionization detector (HP Plot-Q KCl column, 0.53 mm inner diameter (ID) \times 30 m \times 40 μm film, Agilent). Dimethyl ether and water were the only products observed on all catalysts under all conditions. Methane (25% CH₄ in argon, 99.999%, Indiana Oxygen) was introduced to the reactor effluent stream ($0.083 \text{ cm}^3 \text{ s}^{-1}$) and used as an internal standard. First-order and zero-order rate constants for methanol dehydration were calculated as previously reported.⁴⁸

3. RESULTS AND DISCUSSION

3.1. Synthesis and Bulk Characterization of Borosilicate and Boroaluminosilicate Zeolites. B-Al-MFI (Si/B, Si/Al) and B-MFI (Si/B) samples are denoted by the Si/B and Si/Al

ratios present in their synthesis mixtures. The physiochemical properties and elemental compositions of the B-Al-MFI and B-MFI zeolites crystallized in this study are summarized in Table 1. Micropore volumes calculated from N₂ adsorption isotherms (see Figures S1 and S2, and Section S.1, in the Supporting Information) and XRD patterns (see Figures S3 and S4, and Section S.2, in the Supporting Information) of all samples are consistent with the MFI topology, even after washing solid products in water and removing organic structure directing agents by high-temperature oxidative treatments (853 K), suggesting that any deboronation that may have occurred did not result in detectable structural degradation. The characteristic lengths of B-Al-MFI crystallites were taken as their shortest dimension, estimated from linear averages of crystallite sizes measured via SEM micrographs. B-Al-MFI (2.6, 176) and B-Al-MFI (2.6, 88) crystallites are rectangular prism-shaped and have dimensions of ca. $1.5 \mu\text{m} \times 0.3 \mu\text{m} \times 0.3 \mu\text{m}$ (Figures 1a and 1b, respectively), with solid Si/Al ratios of 142 and 88, respectively (see Table 1). B-Al-MFI (13, 176) and B-Al-MFI (13, 88) crystallites are coffin-shaped and have dimensions of ca. $10 \mu\text{m} \times 10 \mu\text{m} \times 15 \mu\text{m}$ (Figures 1c and 1d, respectively), with solid Si/Al ratios of 153 and 74, respectively (see Table 1). SEM micrographs of B-MFI samples are shown in Figure S5 (and Section S.3) in the Supporting Information. Among the B-Al-MFI samples studied here, solid Si/Al ratios were similar (within 20%) to the molar ratios present in their synthesis solutions, while solid Si/B ratios were similar (Si/B = 30–35; see Table 1) among all samples and higher than Si/B ratios in their synthesis solutions (Si/B = 2.6–13). These findings resemble prior reports of B-Al-MCM-22 with a solid Al content (Si/Al = 27) similar to

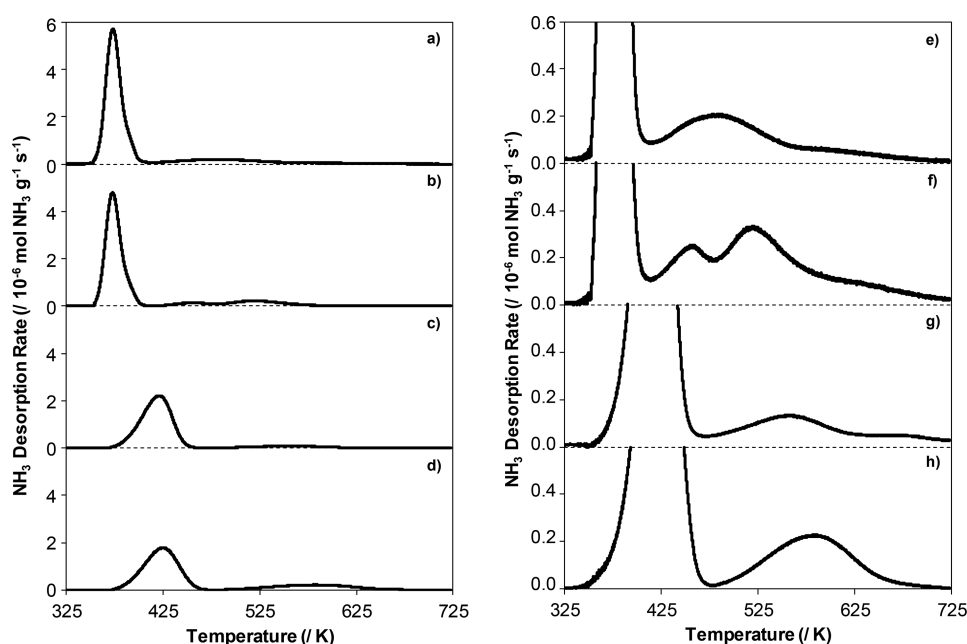


Figure 2. NH_3 desorption rates during TPD of (a) B-Al-MFI (2.6, 176), (b) B-Al-MFI (2.6, 88), (c) B-Al-MFI (13, 176), and (d) B-Al-MFI (13, 88) after saturation in aqueous-phase NH_4NO_3 . Panels (e)–(h) are enlarged views (10 \times magnification of the y-axis) of the same profiles shown in panels (a)–(d), respectively.

Table 2. Quantification of ammonia desorbed during TPD from B-Al-MFI and B-MFI zeolites

sample	Al content ^a ($\times 10^{-3}$ mol g^{-1})	H^+_{Al} ($\times 10^{-3}$ mol g^{-1})			$\text{H}^+/\text{Al}_{\text{tot}}$	
		NH_4^+ aqueous exchange, no He purge	NH_4^+ aqueous exchange, He purge (433 K)	NH_3 gas phase saturation (433 K)	NH_4^+ aqueous exchange, He purge (433 K)	NH_3 gas phase saturation (433 K)
B-Al-MFI (2.6, 176)	0.12	0.86	0.10	0.11	0.90	0.98
B-Al-MFI (2.6, 88)	0.19	0.91	0.20	0.17	1.06	0.90
B-Al-MFI (13, 176)	0.11	0.65	0.08	0.10	0.78	0.94
B-Al-MFI (13, 88)	0.22	0.79	0.16	0.18	0.75	0.83
B-MFI (2.6)	<0.01	0.50	<0.01	<0.01	n.d. ^c	n.d. ^c
B-MFI (13)	<0.01	0.58	<0.01	<0.01	n.d. ^c	n.d. ^c

^aDetermined from atomic absorption spectroscopy. Errors are $\pm 10\%$. ^bErrors for all NH_3 TPD experiments are $\pm 0.03 \times 10^{-3}$ mol NH_3 g^{-1} . ^cNot determined.

that in the synthesis solution ($\text{Si}/\text{Al} = 29$), but with only a partial incorporation of B heteroatoms.¹⁷

Crystallite sizes are primarily influenced by the amount of B present in the synthesis solution under the conditions studied here, reminiscent of reports by Bodart et al.,²⁴ in which the addition of B ($\text{Si}/\text{B} = 12$) to a synthesis solution used to crystallize Al-MFI zeolites ($\text{Si}/\text{Al} = 12$) decreased mean crystallite sizes from 10 μm to 6 μm . We surmise that the smaller B-Al-MFI crystallite sizes obtained here (~ 0.3 μm) reflect, in part, the higher B content used in synthesis mixtures ($\text{Si}/\text{B} = 2.6$). However, we note that the addition of B has also been reported to increase crystallite sizes under certain conditions for borosilicate MFI⁴⁹ and boroaluminosilicate *BEA,²⁹ which likely reflects the influence of other precursors present in synthesis solutions on crystal morphology. Alkanolamines^{50–52} act as chelating agents for Al that delay the release of Al into solution and decrease its incorporation into crystallizing oxide networks (LTA), while ethylenediamine (EDA) acts as a chelating agent for B ($\text{EDA}/\text{B} = 2$)^{53–55} and has been reported to direct the siting of B heteroatoms into straight and sinusoidal

channel locations in MFI.⁵⁵ Alkylamines (e.g., triethylenetetramine,^{22,23,56} ethylenediamine⁵⁷) are also zeolite growth modifiers (ZGMs) that selectively bind to certain zeolite crystal facets during synthesis and influence their aspect ratio. The B-Al-MFI samples in this study were crystallized from solutions containing excess EDA ($\text{B}/\text{EDA} < 2$), which appears to have influenced product crystallite sizes by serving as a ZGM, given that the amount of excess EDA present during synthesis was similar between B-Al-MFI samples that crystallized with similar size and morphology (see Table 1). These synthesis protocols provide a strategy to vary the crystallite size of MFI zeolites independently of Al content, circumventing typical observations of crystallite size that have a tendency to increase with Si/Al ratio.^{19–21}

3.2. Ammonia TPD Methods To Discriminate and Quantify Protons in Boron and Aluminum-Substituted Zeolites. Figure 2 shows the ammonia desorption rate from the four NH_4 -B-Al-MFI samples of varying Al and B content, prepared by liquid-phase NH_4NO_3 ion exchange to saturation at ambient conditions. Multiple desorption features are observed in

each TPD profile, in agreement with previous reports of ammonia desorption from borosilicate MFI zeolites, following the adsorption of gas-phase ammonia at 373 K^{25,39} or 393 K,¹⁷ and in contrast to the single desorption feature observed in TPD from aluminosilicate MFI (see Figure S6 in the Supporting Information). The total amounts of ammonia desorbed from these four $\text{NH}_4\text{-B-Al-MFI}$ samples are listed in Table 2 ($(0.65\text{--}0.91) \times 10^{-3} \text{ mol H}^+ \text{ g}^{-1}$) and overestimated Al contents by a factor of 3–8 (Figure 3), yet were similar to the

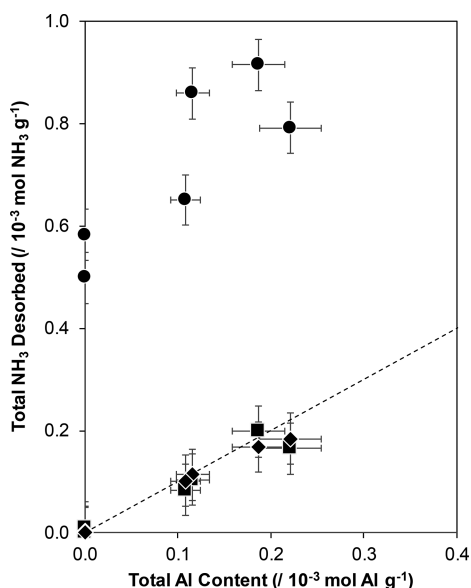


Figure 3. NH_3 desorbed during TPD from B-MFI and B-Al-MFI samples after aqueous-phase NH_4NO_3 saturation (●) without subsequent helium purge, (■) with subsequent helium purge in helium at 433 K, and (◆) with subsequent helium purge in helium after gas phase NH_3 saturation at 433 K. Dashed line represents parity.

total Al and B content ($(0.58\text{--}0.69) \times 10^{-3} \text{ mol g}^{-1}$; see Figure S7 and Table S1, as well as Section S.4, in the Supporting Information). This total reflects ammonia desorption from protons at framework Al and from other binding sites that originate from B, given that TPD after such aqueous-phase NH_4^+ ion-exchange protocols have been shown to detect only Brønsted (but not Lewis) acid sites in aluminosilicate CHA and MFI zeolites.^{34,45}

The lower temperature desorption feature (350–450 K, Figure 2) reflects ammonia desorption from both trigonal and tetrahedral framework boron heteroatoms, each of which can adsorb ammonia.³⁷ B-MFI was synthesized using TEOS as the silicon precursor to avoid adventitious Al impurities often present in colloidal silica,²⁹ and then was subjected to liquid-phase NH_4NO_3 ion exchange to saturation and a subsequent TPD. The TPD profiles of B-MFI (see Figure S8, and Section S.4, in the Supporting Information) show a single desorption feature in a similar low-temperature range, as observed on B-Al-MFI (350–450 K), and the amount of ammonia desorbed from B-MFI ($(0.50\text{--}0.58) \times 10^{-3} \text{ mol H}^+ \text{ g}^{-1}$) is significantly larger than the trace Al contents that were below AAS detection limits ($<10^{-5} \text{ mol g}^{-1}$). However, the lower temperature desorption feature cannot be assigned unambiguously to weaker ammonia binding sites that originate from B heteroatoms, because the position of this feature is influenced by readsorption and diffusion effects that are dependent on crystallite size.^{40,41} This is reflected in the different temperatures corresponding to the

maximum desorption rate of ammonia from $\sim 0.3 \mu\text{m}$ B-Al-MFI crystallites ($\sim 375 \text{ K}$, Figures 2a and 2b) and $\sim 10 \mu\text{m}$ B-Al-MFI crystallites ($\sim 425 \text{ K}$, Figures 2c and 2d), even though these data were collected with identical experimental methods.

These observations of ammonia TPD profiles of B-Al-MFI zeolites after liquid-phase saturation in NH_4NO_3 solution are similar to those reported by Woolery et al. for Al-MFI samples saturated in gas-phase NH_3 at 398 K and purged in dry flowing helium (398 K, 4 h).⁴⁴ Two prominent desorption features at $\sim 493 \text{ K}$ and $\sim 653 \text{ K}$ were assigned to NH_3 desorption from Lewis and Brønsted acid sites, respectively, and overestimated the number of protons (by a factor of 1.3) quantified from peaks in IR spectra for protonated pyridine (1545 cm^{-1}). In contrast, treatment of NH_3 -saturated Al-MFI zeolites in flowing wet helium (398 K) prior to TPD resulted in the disappearance of the lower temperature ($\sim 493 \text{ K}$) desorption feature, and quantification of the NH_3 evolved in the higher temperature feature ($\sim 653 \text{ K}$) was consistent with the number of protons quantified by IR spectroscopy. Thus, purging in wet helium (398 K) was concluded to selectively remove ammonia bound to Lewis acidic Al sites because of competitive adsorption by water, which is a result corroborated by proton site estimates from TPD of samples saturated via aqueous-phase NH_4^+ exchange. Bates³⁴ and Di Iorio⁴⁵ extended these methods to differentiate between Lewis acidic copper (Cu^{2+} , Cu^+) and Brønsted acid sites in partially Cu-exchanged MFI and CHA zeolites, and quantified residual protons by ammonia saturation at elevated temperatures (433 K) and purging treatments in flowing wet helium (433 K) to selectively remove Lewis-bound NH_3 prior to TPD.

We hypothesized that these methods could be adapted to quantify Brønsted acid sites of different strength compensating framework Al and B in borosilicates, given the presence of multiple desorption features in TPD profiles of B-Al-MFI (see Figure 2),^{17,25,39} Al-MFI,⁴⁴ and Cu-exchanged MFI and CHA.^{34,45} The maximum NH_3 desorption rate from B-Al-MFI after liquid-phase NH_4^+ ion exchange was observed at $\sim 375 \text{ K}$ and $\sim 425 \text{ K}$ for samples with characteristic crystallite lengths of 0.3 and $10 \mu\text{m}$, respectively. Based on the methodology used by Bates et al.,³⁴ a purge step in flowing dry helium at a temperature near the maximum desorption rate (433 K) of the low-temperature desorption feature was used here to attempt the selective removal of NH_3 associated with framework B. Water was not required in the intermediate He purge treatment to remove NH_3 from Lewis acid sites, because any Lewis acid sites present were expected to be coordinated to water after aqueous-phase NH_4NO_3 ion exchange.⁴⁴ Rates of ammonia desorption from B-Al-MFI samples after purging in dry helium are shown in Figure 4. For all samples, the low-temperature desorption feature is absent, with a maximum desorption rate observed at $\sim 550 \text{ K}$ in a single primary desorption feature (and a shoulder at higher temperatures). The total amounts of ammonia evolved by this method ($(0.08\text{--}0.20) \times 10^{-3} \text{ mol NH}_3 \text{ g}^{-1}$; see Table 2) for B-Al-MFI samples are similar to their Al content ($\text{H}^+/\text{Al} = 0.75\text{--}1.06$; see Table 2), as shown in Figure 3. Indeed, TPD profiles measured after subjecting NH_3 -saturated B-MFI zeolites to this intermediate helium purge treatment at 433 K show negligible amounts of NH_3 desorbed ($<10^{-5} \text{ mol NH}_3 \text{ g}^{-1}$; see Figure S9 in the Supporting Information). Taken together, these results suggest that NH_3 can be selectively desorbed from B heteroatoms after liquid-phase ion exchange by purging NH_3 -saturated borosilicates in flowing dry helium at 433 K.

Saturation of Cu-exchanged MFI and CHA samples with gaseous NH_3 at 433 K (and subsequent purging in the presence

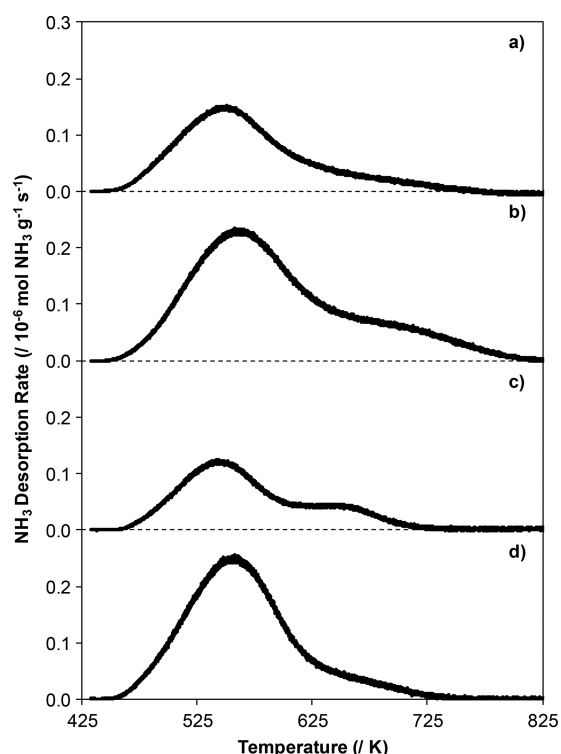


Figure 4. NH_3 desorption rates from (a) B-Al-MFI (2.6, 176), (b) B-Al-MFI (2.6, 88), (c) B-Al-MFI (13, 176), and (d) B-Al-MFI (13, 88) samples after saturation in aqueous-phase NH_4NO_3 and helium purge at 433 K.

of water) has also been used to discriminate between Lewis acidic Cu and Brønsted acid protons,^{34,45} because NH_3 only adsorbs at protons under these conditions. In order to corroborate the number of Brønsted acidic protons at framework Al atoms in borosilicates, a similar gas-phase saturation procedure was performed here (without water) in which H-form B-Al-MFI samples were saturated in a gaseous NH_3 stream (500 ppm of NH_3 in helium) at 433 K (2 h), followed by a purge in flowing dry helium at 433 K (4 h). Rates of NH_3 desorption in a subsequent TPD from B-Al-MFI samples titrated using this method are shown in Figure S10 (as well as Section S.4) in the Supporting Information). On each sample, the total amount of NH_3 evolved is similar to the total Al content ($\text{H}^+/\text{Al} = 0.83\text{--}0.98$; see Table 2) and the amount of NH_3 desorbed after aqueous-phase NH_4^+ -saturation and intermediate He purge, as shown in Figure 3. Again, NH_3 was only desorbed in trace quantities ($<10^{-5}$ mol $\text{NH}_3 \text{ g}^{-1}$) from B-MFI zeolites after this procedure (see Figure S11, as well as Section S.4, in the Supporting Information), verifying that the NH_3 desorbed from B-Al-MFI samples titrated with this procedure originated from H^+ associated with framework Al (H^+_{Al}). The amount of B in B-Al-MFI samples can be estimated from the difference between the NH_3 evolved in TPD after liquid-phase ion exchange in NH_4NO_3 , without and with purging in helium at 433 K (see Figure S12, as well as Section S.4, in the Supporting Information). Next, we use methanol dehydration to dimethyl ether as a catalytic probe reaction to verify that these TPD protocols have accurately distinguished protons at framework Al and B.

3.3. Catalytic Rates of Methanol Dehydration to Dimethyl Ether on Borosilicates. Methanol dehydration to dimethyl ether (DME) can proceed via associative or dissociative routes on solid Brønsted acids (e.g., polyoxometalate

clusters, zeolites).²⁷ In the associative mechanism, methanol monomers form via adsorption of gas-phase methanol at a proton site, and a protonated dimer is formed via adsorption of a second methanol molecule that causes transfer of the proton from the oxide lattice. The protonated dimer then rearranges and dehydrates to form water and an adsorbed DME, which desorbs to regenerate the acid site. Periodic density functional theory (DFT) calculations have shown that methanol monomers and protonated dimers are the most abundant reactive intermediates (MARI) during methanol dehydration catalysis (433 K, >0.2 kPa CH_3OH) on polyoxometalate clusters and Al-*BEA zeolites, giving rise to the following rate expression:²⁷

$$r = \frac{k_{\text{first,A}} P_{\text{CH}_3\text{OH}}}{1 + \frac{k_{\text{first,A}}}{k_{\text{zero,A}}} P_{\text{CH}_3\text{OH}}} \quad (1)$$

where $k_{\text{first,A}}$ and $k_{\text{zero,A}}$ are the first-order and zero-order rate constants of methanol dehydration in the associative pathway, respectively. In situ IR spectra of H-form Al-MFI (433 K, 0–15.3 kPa CH_3OH ;⁵⁸ 415 K, 0–22 kPa CH_3OH ⁴⁸) show hydrogen-bonding modes for methanol monomers ($\sim 2380 \text{ cm}^{-1}$) and protonated dimers ($\sim 2620 \text{ cm}^{-1}$) present in both associative and dissociative pathways, but no peaks for surface methoxy species ($\sim 1457 \text{ cm}^{-1}$) involved in the dissociative mechanism.²⁷ Periodic DFT methods (vdW-DF functional) have estimated free-energy barriers that are $\sim 40 \text{ kJ mol}^{-1}$ lower for the associative than the dissociative pathway at Brønsted acid protons at four different T-sites in Al-MFI channels and intersections (415 K, 10 kPa CH_3OH).⁵⁹ These results collectively indicate that the associative pathway is the predominant mechanism on Al-MFI zeolites under the conditions studied here.

First-order methanol dehydration rate constants reflect free-energy differences between the DME formation transition state and an adsorbed methanol monomer and one gaseous methanol molecule, while zero-order rate constants reflect free-energy differences between the same transition state and protonated methanol dimers. Zero-order rate constants are primarily sensitive to acid strength and are weakly dependent on the local confining environment, because van der Waals interactions with lattice oxygen atoms stabilize the similarly sized transition state and the protonated dimer to similar extents.^{27,60} First-order rate constants are dependent on both acid strength and confinement, which preferentially stabilizes larger DME formation transition states over smaller methanol monomers.^{26,60} Previous data collected from our group⁴⁸ has shown quantitative agreement in first-order and zero-order rate constants (per H^+_{Al} , 415 K), and corresponding activation enthalpy and entropy values, with values of rate constants and activation parameters reported by Jones et al. (per H^+_{Al} , 433 K)²⁶ on a suite of commercially available Al-MFI zeolites of different Si/Al ratio. Methanol dehydration turnover rates (per H^+ , 433 K, 0.2–20 kPa) are two orders of magnitude lower on B-MFI than on Al-MFI, reflecting deprotonation energies that are $\sim 70 \text{ kJ mol}^{-1}$ higher for protons at framework B than Al.²⁶ Thus, methanol dehydration turnover rates measured in zero-order regimes on B-Al-MFI zeolites should be dependent predominantly on the number of protons at framework Al in B-Al-MFI.

DME formation rates (per H^+_{Al} , 415 K) on the four B-Al-MFI samples, normalized by the number of protons compensating framework Al as quantified by the selective NH_3 titration methods reported here (H^+_{Al} ; see Table 2), are shown as a function of methanol partial pressure in Figure 5. DME

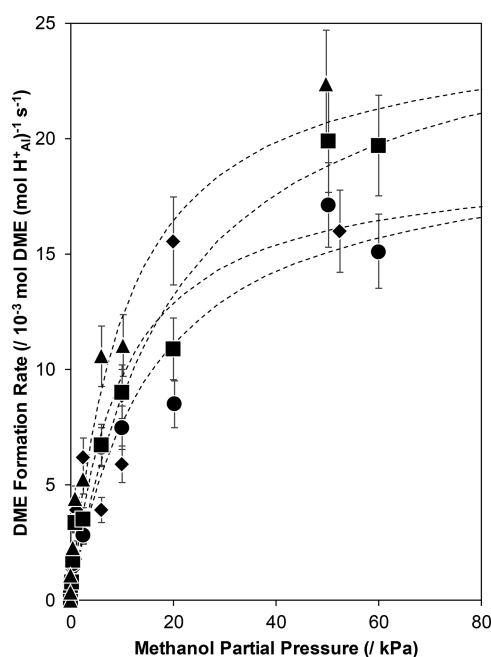


Figure 5. DME formation rates on (◆) B-Al-MFI (2.6, 176), (●) B-Al-MFI (2.6, 88), (■) B-Al-MFI (13, 176), and (▲) B-Al-MFI (13, 88) samples at 415 K. Rates are normalized by the number of protons at framework Al (H^+_{Al}) quantified by NH_3 TPD after aqueous-phase saturation in NH_4NO_3 and intermediate purging in helium at 433 K (see Table 2).

formation rates on B-Al-MFI zeolites increased linearly at low methanol partial pressures (<2 kPa) and approached a zero-order kinetic regime at higher pressures (>40 kPa), in agreement with previous reports on Al-MFI zeolites under similar conditions (433 K, 0–20 kPa CH_3OH ;²⁶ 415 K, 0–60 kPa CH_3OH ;⁴⁸). These data were regressed to eq 1 to estimate zero-order and first-order rate constants, which are shown in Figure 6, as a function of H^+_{Al} content on the B-Al-MFI samples, along with data reported previously on Al-MFI samples. Zero-order rate constants are identical, within experimental error, for all B-Al-MFI samples ($(20\text{--}26) \times 10^{-3}$ mol DME (mol H^+_{Al})⁻¹ s⁻¹, Figure 6) and in quantitative agreement with values reported previously by Jones et al.²⁶ and Di Iorio et al.⁴⁸ on Al-MFI zeolites. In addition, zero-order DME formation rates (per g) are independent of the number of B heteroatoms present (see Figure S13, as well as Section S.5, in the Supporting Information), in agreement with previous reports for a variety of acid-catalyzed reactions in B-Al-MFI (*n*-hexane cracking,²⁸ ethylbenzene dealkylation,²⁸ cyclopropane isomerization,²⁸ and ethylene methylation²⁵), and DME formation rates measured on B-MFI (13) suggest that B contributes to <1% of measured rates on B-Al-MFI samples (see Figure S14, as well as Section S.5, in the Supporting Information). These results collectively provide rigorous verification that the ammonia titration methods developed here quantify only catalytically relevant Brønsted acid protons in B-Al-MFI zeolites of varying B (Si/B = 20–35) and Al (Si/Al = 74–153) heteroatom content and diffusion parameters ($\Psi = 0.02\text{--}42$ mol H^+ nm⁻¹, Table 1).

First-order rate constants (per H^+_{Al} , 415 K; Figure 6) for the B-Al-MFI samples ($1.3\text{--}2.4 \times 10^{-3}$ mol DME (mol H^+_{Al})⁻¹ kPa⁻¹ s⁻¹) are lower, by a factor of 2–10, than those reported previously for Al-MFI ($(4\text{--}12) \times 10^{-3}$ mol DME (mol H^+_{Al})⁻¹ kPa⁻¹ s⁻¹, 433 K;²⁶ $(4\text{--}16) \times 10^{-3}$ mol DME (mol H^+_{Al})⁻¹ kPa⁻¹ s⁻¹, 415 K⁴⁸). Intraparticle mass-transfer limitations can decrease

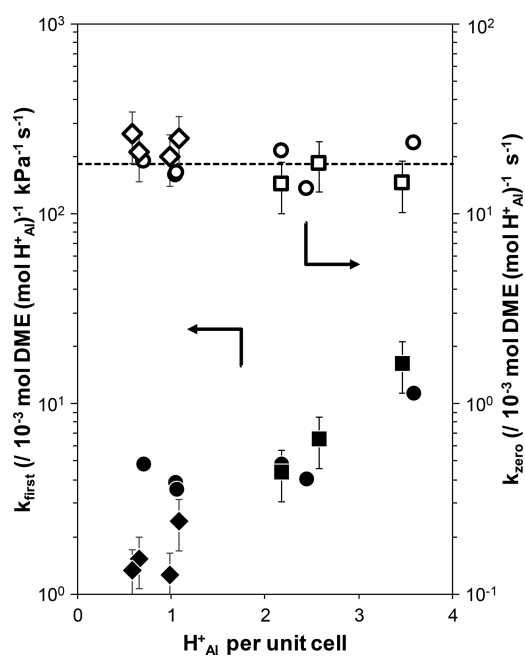


Figure 6. First-order (closed symbols) and zero-order (open symbols) rate constants of methanol dehydration on Al-MFI samples reported by (●) Jones et al.²⁶ at 433 K, (■) Di Iorio et al.⁴⁸ at 415 K, and (◆) in this study on B-Al-MFI samples at 415 K.

observed rates measured in positive-order kinetic regimes by decreasing reactant concentrations at active sites,⁶¹ as previously reported during methanol dehydration catalysis (415 K) in large Al-CHA crystallites (Si/Al = 27, 6 μ m, $\Psi = 50$ mol H^+ nm⁻¹).⁴⁸ Intraparticle methanol concentration gradients were estimated in the four B-Al-MFI zeolites under the conditions studied for methanol dehydration catalysis (see Figures S15–S18, as well as Section S.6, in the Supporting Information) using methods reported previously.⁴⁸ Methanol partial pressures decrease by less than 15% from the bulk external fluid to the center of catalyst particles in all B-Al-MFI zeolites, with effectiveness factors near unity (see Figure S19, as well as Section S.6, in the Supporting Information) that were estimated using the first-order rate constants and the physiochemical properties in Table 1 (additional details are given in Section S.6 in the Supporting Information).

Differences in first-order methanol dehydration rate constants among microporous aluminosilicates, when rigorously of kinetic origin, reflect differences in the stabilization of larger DME formation transition states and smaller methanol monomers by van der Waals interactions, which cause rate constants to increase as confining voids become smaller.⁶⁰ First-order rate constant values of $\sim 7.0 \times 10^{-3}$ mol DME (mol H^+_{Al})⁻¹ kPa⁻¹ s⁻¹ are characteristic of protons confined within pores of ~ 0.6 nm diameter, while values of $\sim 2.0 \times 10^{-3}$ mol DME (mol H^+_{Al})⁻¹ kPa⁻¹ s⁻¹ are characteristic of protons confined within ~ 0.8 nm voids.⁶⁰ The lower first-order methanol dehydration rate constants measured on B-Al-MFI (Figure 6) may reflect the preferential siting of framework Al into T-sites located within MFI intersections (~ 0.7 nm voids¹²) over those in straight and sinusoidal channels (~ 0.55 nm voids¹²), which seems plausible, considering that EDA chelates with B during conditions of synthesis (B/EDA = 2)⁵³ and has been characterized by XRD to locate within straight and sinusoidal channels during synthesis of B-MFI.⁵⁵ Although first-order rate constant values of $\sim 5 \times 10^{-3}$

mol DME (mol H_{Al}^+)⁻¹ kPa⁻¹ s⁻¹ have been attributed previously to protons confined within MFI intersections, these materials were synthesized in the presence of both TPA⁺ and Na⁺ cations,²⁶ which are synthetic mixtures that have been reported by Yokoi et al. to incorporate Al at T-sites both in MFI intersections and in straight and sinusoidal channels.⁶² The first-order rate constant values measured here, which are consistent with values expected for protons confined within ~0.7–0.8 nm voids characteristic of MFI intersections,^{12,60} suggest that B-Al-MFI zeolites synthesized in the presence of EDA and TPA⁺ may contain Al preferentially sited at T-sites located within MFI intersections.

4. CONCLUSIONS

Ammonia titration methods were developed to distinguish between framework B and Al heteroatoms in boroaluminosilicate MFI catalysts, where the latter generate protons that are stronger acids and behave as dominant active sites for Brønsted acid-catalyzed reactions. Temperature-programmed desorption (TPD) of ammonia following aqueous-phase NH₄⁺ ion exchange quantifies both framework Al and B species in B-Al-MFI. Intermediate treatments to remove weakly bound ammonia at framework B sites (flowing dry helium, 433 K) or gas-phase NH₃ saturation at intermediate temperatures (433 K), however, quantify only protons that charge compensate framework Al atoms. These methods should be adaptable to discriminate and quantify weaker and stronger protons respectively originating from B and Al in other boroaluminosilicates, and are especially useful to quantify catalytically relevant protons in small-pore or Al-rich molecular sieves.^{32,34}

The number of protons counted by these TPD methods agreed quantitatively with the amount of total Al measured by atomic absorption spectroscopy ($H^+/Al = 0.75\text{--}1.06$) on a series of B-Al-MFI zeolites of varying crystallite size and Al contents. Crystallite sizes (0.3–10 μm) and Si/Al ratios (74–153) were independently varied in B-Al-MFI zeolites synthesized in the presence of tetrapropylammonium cation and ethylenediamine structure directing agents, resulting in crystallites with diffusion parameters that varied by 3 orders of magnitude (0.02–42 mol H_{Al}^+ nm⁻¹). These findings differ from heuristic guidelines that crystallite sizes and Al contents are correlated structural properties for aluminosilicates synthesized hydrothermally, and the typical observations that crystallite sizes increase with Si/Al ratios, which likely reflects the dual roles of ethylenediamine as a structure directing agent and a zeolite growth modifier during MFI crystallization. The ability to vary Si/Al ratios and crystallite sizes over a range of diffusion parameters allows for independent assessments of how these properties influence rates and selectivities of catalytic reaction networks, especially where catalytic and transport phenomena are inherently coupled, such as in alkene oligomerization¹² and methanol-to-olefins^{8,9} cycles.

The number of protons compensating framework Al atoms were used to rigorously normalize zero-order rate constants for methanol dehydration to dimethyl ether, a catalytic probe that is sensitive to Brønsted acid strength and able to unambiguously discriminate contributions from protons that charge-compensate Al and B heteroatoms. We surmise that first-order dehydration rate constants (per H_{Al}^+ , 415 K) on B-Al-MFI samples that are lower than values characteristic of Al-MFI zeolites may reflect the preferential siting of Al in T-sites located in MFI intersections, wherein preferential stabilization of larger DME formation transition states, relative to smaller methanol precursors by van der Waals interactions, is less effective than within smaller MFI

channels. Zero-order dehydration rate constants (per H_{Al}^+ , 415 K) were identical on all B-Al-MFI zeolites with varying crystallite size and Al content, and were similar to values characteristic of Al-MFI zeolites,^{26,48} providing confirmation that the NH₃ titration and TPD methods developed here selectively quantify protons at Al atoms, as required for rigorous normalization of turnover rates. These findings are consistent with prior reports of rates for Brønsted acid-catalyzed reactions on borosilicates that are solely dependent on the residual trace Al content, which is often present as adventitious impurities introduced from inorganic precursors used in zeolite crystallization or from contact with binders in formulated catalytic solids.

■ ASSOCIATED CONTENT

■ Supporting Information

The Supporting Information is available free of charge on the ACS Publications website at DOI: 10.1021/acs.iecr.8b00933.

Nitrogen adsorption isotherms, X-ray diffraction patterns, scanning electron micrographs, supplemental NH₃ TPD profiles, methanol dehydration rates on B-MFI, and assessment of intraparticle transport artifacts during methanol dehydration catalysis in B-Al-MFI samples (PDF)

■ AUTHOR INFORMATION

Corresponding Author

*E-mail: rgounder@purdue.edu.

ORCID

Rajamani Gounder: 0000-0003-1347-534X

Notes

The authors declare no competing financial interest.

Biographies



Phil Kester is a 4th year Ph.D. student in Prof. Raj Gounder's research group, and he currently serves as the Chair of the Student Leadership Council of the NSF Engineering Research Center for the Innovative and Strategic Transformation of Alkane Resources (CISTAR). His research in CISTAR is focused on determining the kinetic and mechanistic roles of Brønsted and Lewis acid active site location and proximity in molecular sieves for reactions of light hydrocarbons.



Jeff Miller is a Professor in Purdue's Davidson School of Chemical Engineering, and a research thrust lead in CISTAR. His research interests include development and in situ synchrotron characterizations of new catalysts for conversion of abundant shale gas hydrocarbons to fuels and chemicals. Prior to joining Purdue in 2015, he was the Catalysis Group Leader at Argonne National Laboratory's Chemical Sciences and Engineering Division. Prior to joining Argonne, he worked for the Amoco Oil Company (now BP) for more than 27 years.



Raj Gounder is currently the Larry and Virginia Faith Assistant Professor in the Davidson School of Chemical Engineering at Purdue University. He is a Research Thrust co-lead in CISTAR. He leads an experimental research group that studies the catalysis of energy and the environment, focusing on converting conventional and emerging carbon feedstocks to fuels and chemicals, and on automotive pollution abatement.

ACKNOWLEDGMENTS

We thank YoonRae Cho for assistance with zeolite synthesis, Dr. Young Gul Hur for assistance with SEM imaging, and Claire Nimlos and John Di Iorio for assistance collecting methanol dehydration kinetic data. We also thank John, Claire, and Young for technical discussions and feedback on this manuscript. We acknowledge the support for this work provided by the National Science Foundation under Cooperative Agreement No. EEC-1647722, an Engineering Research Center for the Innovative and Strategic Transformation of Alkane Resources (CISTAR).

REFERENCES

- (1) Corma, A. Inorganic Solid Acids and Their Use in Acid-Catalyzed Hydrocarbon Reactions. *Chem. Rev.* **1995**, 95 (3), 559–614.
- (2) Degnan, T. F. The Implications of the Fundamentals of Shape Selectivity for the Development of Catalysts for the Petroleum and Petrochemical Industries. *J. Catal.* **2003**, 216 (1), 32–46.
- (3) Chang, C. D. Hydrocarbons from Methanol. *Catal. Rev.: Sci. Eng.* **1983**, 25 (1), 1–118.
- (4) Tabak, S. A. Oligomerization of Olefins. U.S. Patent No. US4254295A, March 3, 1981.
- (5) Garwood, W. E. Conversion of C₂–C₁₀ to Higher Olefins over Synthetic Zeolite ZSM-5. In *Intrazeolite Chemistry*; ACS Symposium Series, Vol. 218; American Chemical Society: Washington, DC, 1983; pp 383–396.
- (6) Sugimoto, M.; Katsuno, H.; Takatsu, K.; Kawata, N. Correlation between the Crystal Size and Catalytic Properties of ZSM-5 Zeolites. *Zeolites* **1987**, 7 (6), 503–507.
- (7) Choi, M.; Na, K.; Kim, J.; Sakamoto, Y.; Terasaki, O.; Ryoo, R. Stable Single-Unit-Cell Nanosheets of Zeolite MFI as Active and Long-Lived Catalysts. *Nature* **2009**, 461 (7261), 246–249.
- (8) Khare, R.; Millar, D.; Bhan, A. A Mechanistic Basis for the Effects of Crystallite Size on Light Olefin Selectivity in Methanol-to-Hydrocarbons Conversion on MFI. *J. Catal.* **2015**, 321, 23–31.
- (9) Khare, R.; Liu, Z.; Han, Y.; Bhan, A. A Mechanistic Basis for the Effect of Aluminum Content on Ethene Selectivity in Methanol-to-Hydrocarbons Conversion on HZSM-5. *J. Catal.* **2017**, 348, 300–305.
- (10) Corma, A.; Martínez, C.; Dorskocil, E. Designing MFI-Based Catalysts with Improved Catalyst Life for Oligomerization to High-Quality Liquid Fuels. *J. Catal.* **2013**, 300, 183–196.
- (11) Popov, A. G.; Pavlov, V. S.; Ivanova, I. I. Effect of Crystal Size on Butenes Oligomerization over MFI Catalysts. *J. Catal.* **2016**, 335, 155–164.
- (12) Sarazen, M. L.; Dorskocil, E.; Iglesia, E. Effects of Void Environment and Acid Strength on Alkene Oligomerization Selectivity. *ACS Catal.* **2016**, 6 (10), 7059–7070.
- (13) Knott, B. C.; Nimlos, C. T.; Robichaud, D. J.; Nimlos, M. R.; Kim, S.; Gounder, R. Consideration of the Aluminum Distribution in Zeolites in Theoretical and Experimental Catalysis Research. *ACS Catal.* **2018**, 8 (2), 770–784.
- (14) Sarazen, M. L.; Dorskocil, E.; Iglesia, E. Catalysis on Solid Acids: Mechanism and Catalyst Descriptors in Oligomerization Reactions of Light Alkenes. *J. Catal.* **2016**, 344, 553–569.
- (15) Bjørgen, M.; Svelle, S.; Joensen, F.; Nerlov, J.; Kolboe, S.; Bonino, F.; Palumbo, L.; Bordiga, S.; Olsbye, U. Conversion of Methanol to Hydrocarbons over Zeolite H-ZSM-5: On the Origin of the Olefinic Species. *J. Catal.* **2007**, 249 (2), 195–207.
- (16) Liang, T.; Chen, J.; Qin, Z.; Li, J.; Wang, P.; Wang, S.; Wang, G.; Dong, M.; Fan, W.; Wang, J. Conversion of Methanol to Olefins over H-ZSM-5 Zeolite: Reaction Pathway Is Related to the Framework Aluminum Siting. *ACS Catal.* **2016**, 6 (11), 7311–7325.
- (17) Chen, J.; Liang, T.; Li, J.; Wang, S.; Qin, Z.; Wang, P.; Huang, L.; Fan, W.; Wang, J. Regulation of Framework Aluminum Siting and Acid Distribution in H-MCM-22 by Boron Incorporation and Its Effect on the Catalytic Performance in Methanol to Hydrocarbons. *ACS Catal.* **2016**, 6 (4), 2299–2313.
- (18) Dědeček, J.; Sobalík, Z.; Wichterlová, B. Siting and Distribution of Framework Aluminium Atoms in Silicon-Rich Zeolites and Impact on Catalysis. *Catal. Rev.: Sci. Eng.* **2012**, 54 (2), 135–223.
- (19) Shirazi, L.; Jamshidi, E.; Ghasemi, M. R. The Effect of Si/Al Ratio of ZSM-5 Zeolite on Its Morphology, Acidity and Crystal Size. *Cryst. Res. Technol.* **2008**, 43 (12), 1300–1306.
- (20) Kim, W. J.; Lee, M. C.; Hayhurst, D. T. Synthesis of ZSM-5 at Low Temperature and Atmospheric Pressure in a Pilot-Scale Batch Reactor. *Microporous Mesoporous Mater.* **1998**, 26 (1), 133–141.
- (21) Armaroli, T.; Simon, L. J.; Digne, M.; Montanari, T.; Bevilacqua, M.; Valtchev, V.; Patarin, J.; Busca, G. Effects of Crystal Size and Si/Al Ratio on the Surface Properties of H-ZSM-5 Zeolites. *Appl. Catal., A* **2006**, 306, 78–84.
- (22) Lupulescu, A. I.; Rimer, J. D. Tailoring Silicalite-1 Crystal Morphology with Molecular Modifiers. *Angew. Chem., Int. Ed.* **2012**, 51 (14), 3345–3349.
- (23) Lupulescu, A. I.; Kumar, M.; Rimer, J. D. A Facile Strategy To Design Zeolite L Crystals with Tunable Morphology and Surface Architecture. *J. Am. Chem. Soc.* **2013**, 135 (17), 6608–6617.

- (24) Bodart, P.; Nagy, J. B.; Gabelica, Z.; Derouane, E. G. Competitive Lattice Incorporation of Aluminium and Boron during Crystallization of ZSM-5 Type Zeolites. *Appl. Catal.* **1986**, *24* (1), 315–318.
- (25) Zhu, Q.; Kondo, J. N.; Yokoi, T.; Setoyama, T.; Yamaguchi, M.; Takewaki, T.; Domen, K.; Tatsumi, T. The Influence of Acidities of Boron- and Aluminium-Containing MFI Zeolites on Co-Reaction of Methanol and Ethene. *Phys. Chem. Chem. Phys.* **2011**, *13* (32), 14598–14605.
- (26) Jones, A. J.; Carr, R. T.; Zones, S. I.; Iglesia, E. Acid Strength and Solvation in Catalysis by MFI Zeolites and Effects of the Identity, Concentration and Location of Framework Heteroatoms. *J. Catal.* **2014**, *312*, 58–68.
- (27) Carr, R. T.; Neurock, M.; Iglesia, E. Catalytic Consequences of Acid Strength in the Conversion of Methanol to Dimethyl Ether. *J. Catal.* **2011**, *278* (1), 78–93.
- (28) Chu, C. T.-W.; Kuehl, G. H.; Lago, R. M.; Chang, C. D. Isomorphous Substitution in Zeolite Frameworks: II. Catalytic Properties of [B]ZSM-5. *J. Catal.* **1985**, *93* (2), 451–458.
- (29) Derewinski, M.; Renzo, F. D.; Espiau, P.; Fajula, F.; Nicolle, M.-A. Synthesis of Zeolite Beta in Boron–Aluminium Media. In *Zeolite Chemistry and Catalysis*; Jacobs, P. A.; Jaeger, N. I.; Kubelková, L.; Wichterlová, B., Eds.; Studies in Surface Science and Catalysis, Vol. 69; Elsevier: Amsterdam, 1991; pp 127–134.
- (30) Shihabi, D. S.; Garwood, W. E.; Chu, P.; Miale, J. N.; Lago, R. M.; Chu, C. T.-W.; Chang, C. D. Aluminum Insertion into High-Silica Zeolite Frameworks: II. Binder Activation of High-Silica ZSM-5. *J. Catal.* **1985**, *93* (2), 471–474.
- (31) Gabelica, Z.; Nagy, J. B.; Bodart, P.; Debras, G. High Resolution Solid State MAS ^{11}B -NMR Evidence of Boron Incorporation in Tetrahedral Sites of Zeolites. *Chem. Lett.* **1984**, *13* (7), 1059–1062.
- (32) Biaglow, A. I.; Parrillo, D. J.; Kokotailo, G. T.; Gorte, R. J. A Study of Dealuminated Faujasites. *J. Catal.* **1994**, *148* (1), 213–223.
- (33) Gounder, R.; Jones, A. J.; Carr, R. T.; Iglesia, E. Solvation and Acid Strength Effects on Catalysis by Faujasite Zeolites. *J. Catal.* **2012**, *286*, 214–223.
- (34) Bates, S. A.; Delgass, W. N.; Ribeiro, F. H.; Miller, J. T.; Gounder, R. Methods for NH_3 Titration of Brønsted Acid Sites in Cu-Zeolites That Catalyze the Selective Catalytic Reduction of NO_x with NH_3 . *J. Catal.* **2014**, *312*, 26–36.
- (35) Hwang, S.-J.; Chen, C.-Y.; Zones, S. I. Boron Sites in Borosilicate Zeolites at Various Stages of Hydration Studied by Solid State NMR Spectroscopy. *J. Phys. Chem. B* **2004**, *108* (48), 18535–18546.
- (36) Coudurier, G.; Védre, J. C. Catalytic and Acidic Properties of Boron Pentasil Zeolites. In *New Developments in Zeolite Science and Technology*; Murakami, Y.; Iijima, A.; Ward, J. W., Eds.; Studies in Surface Science and Catalysis, Vol. 28; Elsevier: Amsterdam, 1986; pp 643–652.
- (37) Sayed, M. B.; Auroux, A.; Védre, J. C. The Effect of Boron on ZSM-5 Zeolite Shape Selectivity and Activity: II. Coincorporation of Aluminium and Boron in the Zeolite Lattice. *J. Catal.* **1989**, *116* (1), 1–10.
- (38) Scholle, K. F. M. G. J.; Kentgens, A. P. M.; Veeman, W. S.; Frenken, P.; Van der Velden, G. P. M. Proton Magic Angle Spinning Nuclear Magnetic Resonance and Temperature Programmed Desorption Studies of Ammonia on the Acidity of the Framework Hydroxyl Groups in the Zeolite H-ZSM-5 and in H-Boralite. *J. Phys. Chem.* **1984**, *88* (1), 5–8.
- (39) Xu, W. Q.; Suib, S. L.; O'Young, C. L. Studies of Acidic Sites on Boralites by Temperature-Programmed Desorption (TPD) of NH_3 , C_2H_4 , and $1\text{-C}_4\text{H}_8$. *J. Catal.* **1993**, *144* (1), 285–295.
- (40) Gorte, R. J. Design Parameters for Temperature Programmed Desorption from Porous Catalysts. *J. Catal.* **1982**, *75* (1), 164–174.
- (41) Demmin, R. A.; Gorte, R. J. Design Parameters for Temperature-Programmed Desorption from a Packed Bed. *J. Catal.* **1984**, *90* (1), 32–39.
- (42) Kofke, T. J. G.; Gorte, R. J.; Kokotailo, G. T. Stoichiometric Adsorption Complexes in [B]- and [Fe]-ZSM-5 Zeolites. *J. Catal.* **1989**, *116* (1), 252–262.
- (43) Parrillo, D. J.; Adamo, A. T.; Kokotailo, G. T.; Gorte, R. J. Amine Adsorption in H-ZSM-5. *Appl. Catal.* **1990**, *67* (1), 107–118.
- (44) Woolery, G. L.; Kuehl, G. H.; Timken, H. C.; Chester, A. W.; Vartuli, J. C. On the Nature of Framework Brønsted and Lewis Acid Sites in ZSM-5. *Zeolites* **1997**, *19* (4), 288–296.
- (45) Di Iorio, J. R.; Bates, S. A.; Verma, A. A.; Delgass, W. N.; Ribeiro, F. H.; Miller, J. T.; Gounder, R. The Dynamic Nature of Brønsted Acid Sites in Cu-Zeolites During NO_x Selective Catalytic Reduction: Quantification by Gas-Phase Ammonia Titration. *Top. Catal.* **2015**, *58* (7–9), 424–434.
- (46) Borghard, W. S.; Reischman, P. T.; Sheppard, E. W. Argon Sorption in ZSM-5. *J. Catal.* **1993**, *139* (1), 19–23.
- (47) Borghard, W. S.; Sheppard, E. W.; Schoennagel, H. J. An Automated, High Precision Unit for Low-pressure Physisorption. *Rev. Sci. Instrum.* **1991**, *62* (11), 2801–2809.
- (48) Di Iorio, J. R.; Nimlos, C. T.; Gounder, R. Introducing Catalytic Diversity into Single-Site Chabazite Zeolites of Fixed Composition via Synthetic Control of Active Site Proximity. *ACS Catal.* **2017**, *7* (10), 6663–6674.
- (49) Cichocki, A.; Parasiewicz-Kaczmarek, J.; Michalik, M.; Buś, M. Synthesis and Characterization of Boralites with the MFI Structure. *Zeolites* **1990**, *10* (6), 577–582.
- (50) Scott, G.; Thompson, R. W.; Dixon, A. G.; Sacco, A. The Role of Triethanolamine in Zeolite Crystallization. *Zeolites* **1990**, *10* (1), 44–50.
- (51) Morris, M.; Sacco, A.; Dixon, A. G.; Thompson, R. W. The Role of an Aluminum-Tertiary. *Zeolites* **1991**, *11* (2), 178–183.
- (52) Morris, M.; Dixon, A. G.; Sacco, A.; Thompson, R. W. Investigations on the Relative Effectiveness of Some Tertiary Alkanolamines in the Synthesis of Large-Crystal Zeolite NaA. *Zeolites* **1993**, *13* (2), 113–121.
- (53) Gies, H.; Gunawardane, R. P. One-Step Synthesis, Properties and Crystal Structure of Aluminium-Free Ferrierite. *Zeolites* **1987**, *7* (5), 442–445.
- (54) Perego, G.; Bellussi, G.; Millini, R.; Alberti, A.; Zanardi, S. B-Containing Molecular Sieves Crystallized in the Presence of Ethylenediamine. Part I: Crystal Structure of as-Synthesized B-FER. *Microporous Mesoporous Mater.* **2002**, *56* (2), 193–202.
- (55) Perego, G.; Bellussi, G.; Millini, R.; Alberti, A.; Zanardi, S. B-Containing Molecular Sieves Crystallized in the Presence of Ethylenediamine. Part II: Crystal Structure of as-Synthesized B-MFI. *Microporous Mesoporous Mater.* **2003**, *58* (3), 213–223.
- (56) Karimi, R.; Bayati, B.; Charchi Aghdam, N.; Ejtemaei, M.; Babaluo, A. A. Studies of the Effect of Synthesis Parameters on ZSM-5 Nanocrystalline Material during Template-Hydrothermal Synthesis in the Presence of Chelating Agent. *Powder Technol.* **2012**, *229*, 229–236.
- (57) Rimer, J. D. Zeolite Compositions and Methods for Tailoring Zeolite Crystal Habits with Growth Modifiers. World Patent No. WO2012106675A2, Aug. 9, 2012.
- (58) Jones, A. J.; Iglesia, E. Kinetic, Spectroscopic, and Theoretical Assessment of Associative and Dissociative Methanol Dehydration Routes in Zeolites. *Angew. Chem.* **2014**, *126* (45), 12373–12377.
- (59) Ghorbanpour, A.; Rimer, J. D.; Grabow, L. C. Computational Assessment of the Dominant Factors Governing the Mechanism of Methanol Dehydration over H-ZSM-5 with Heterogeneous Aluminum Distribution. *ACS Catal.* **2016**, *6* (4), 2287–2298.
- (60) Jones, A. J.; Zones, S. I.; Iglesia, E. Implications of Transition State Confinement within Small Voids for Acid Catalysis. *J. Phys. Chem. C* **2014**, *118* (31), 17787–17800.
- (61) Weisz, P. B.; Prater, C. D. Interpretation of Measurements in Experimental Catalysis. *Adv. Catal.* **1954**, *6*, 143–196.
- (62) Yokoi, T.; Mochizuki, H.; Namba, S.; Kondo, J. N.; Tatsumi, T. Control of the Al Distribution in the Framework of ZSM-5 Zeolite and Its Evaluation by Solid-State NMR Technique and Catalytic Properties. *J. Phys. Chem. C* **2015**, *119* (27), 15303–15315.